Biogeosciences, 10, 6339–6355, 2013
www.biogeosciences.net/10/6339/2013/
doi:10.5194/bg-10-6339-2013

Biogeosciences Open Access

Physical and biogeochemical forcing of oxygen and nitrate changes during El Niño/El Viejo and La Niña/La Vieja upper-ocean phases in the tropical eastern South Pacific along 86° W

P. J. Llanillo[1], **J. Karstensen**[2], **J. L. Pelegrí**[1], **and L. Stramma**[2]

[1]LINCGlobal, Institut de Ciències del Mar, CSIC, Passeig Maritim de la Barceloneta 37–49, 08003 Barcelona, Spain
[2]GEOMAR Helmholtz Centre for Ocean Research Kiel, Düsternbrooker Weg 20, 24105 Kiel, Germany

Correspondence to: P. J. Llanillo (llanillo@icm.csic.es)

Received: 30 September 2012 – Published in Biogeosciences Discuss.: 11 December 2012
Revised: 22 July 2013 – Accepted: 12 August 2013 – Published: 9 October 2013

Abstract. Temporal changes in the water mass distribution and biogeochemical signals in the tropical eastern South Pacific are investigated with the help of an extended optimum multi-parameter (OMP) analysis, a technique for inverse modeling of mixing and biogeochemical processes through a multidimensional least-square fit. Two ship occupations of a meridional section along 85°50′ W from 14° S to 1° N are analysed during relatively warm (El Niño/El Viejo, March 1993) and cold (La Niña/La Vieja, February 2009) upper-ocean phases. The largest El Niño–Southern Oscillation (ENSO) impact was found in the water properties and water mass distribution in the upper 200 m north of 10° S. ENSO promotes the vertical motion of the oxygen minimum zone (OMZ) associated with the hypoxic equatorial subsurface water (ESSW). During a cold phase the core of the ESSW is found at shallower layers, replacing shallow (top 200 m) subtropical surface water (STW). The heave of isopycnals due to ENSO partially explains the intrusion of oxygen-rich and nutrient-poor antarctic intermediate water (AAIW) into the depth range of 150–500 m. The other cause of the AAIW increase at shallower depths is that this water mass flowed along shallower isopycnals in 2009. The shift in the vertical location of AAIW reaching the OMZ induces changes in the amount of oxygen advected and respired inside the OMZ: the larger the oxygen supply, the greater the respiration and the lower the nitrate loss through denitrification. Variations in the intensity of the zonal currents in the equatorial current system, which ventilates the OMZ from the west, are used to explain the patchy latitudinal changes of seawater properties observed along the repeated section. Significant changes reach down to 800 m, suggesting that decadal variability (Pacific decadal oscillation) is also a potential driver in the observed variability.

1 Introduction

Oxygen minimum zones (OMZs) exist with different intensities in the upper thermocline of the eastern part of the subtropical gyres of the Pacific and Atlantic oceans as well as in the northern Indian Ocean (Karstensen et al., 2008; Paulmier and Ruiz-Pino, 2009). When dissolved oxygen falls below a certain critical level, widespread mortality or avoidance of affected areas will result (Vaquer-Sunyer and Duarte, 2008). Expansion of the OMZs will narrow down the habitable depth range of fishes and, along with overfishing, may threaten the sustainability of pelagic fisheries and marine ecosystems (e.g. Stramma et al., 2012). Decreasing oxygen concentrations and OMZ expansion have been found for all tropical oceans (Stramma et al., 2008, 2010b), perhaps as part of long-term decadal type variability (Deutsch et al., 2011). However, increasing oxygen content has been reported as occurring between 200 m and 700 m south of 15° S in the Pacific (Stramma et al., 2010b). The characteristics and variability of the OMZs are driven by physical and biological processes. Because of the upwelling of nutrient-rich waters in the eastern boundary regions, the waters overlying the eastern South Pacific OMZ belong to the most productive areas in the world ocean (Strub et al., 1998).

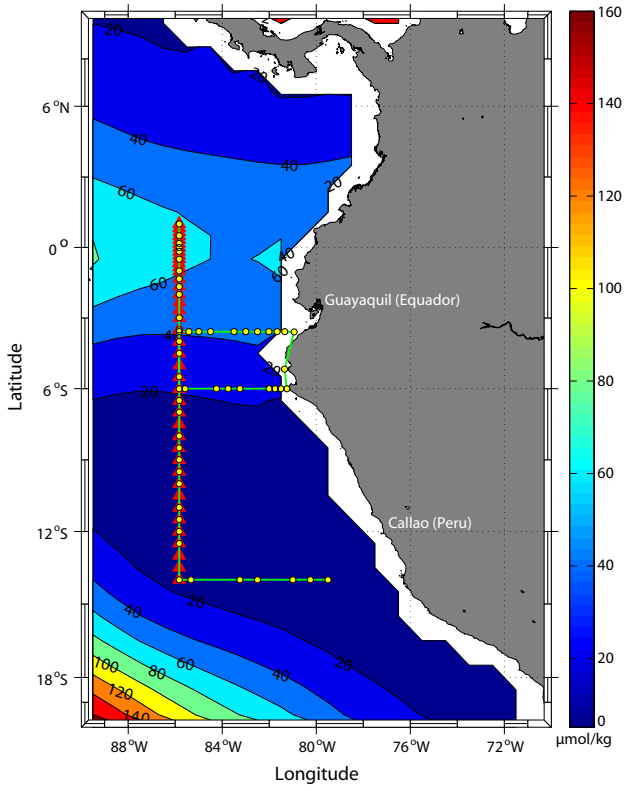

Fig. 1a. Map of the study area with the track (green line) of the Meteor M77 cruise (February 2009) and stations between 14° S and 1° N (red triangles) of the WOCE P19 cruise (March 1993). The yellow dots indicate the rosette stations of the M77 cruise selected for the extended OMP analysis. The background shows the climatological mean of dissolved oxygen (µmol kg^{-1}) at 200 dbar from the World Ocean Atlas 2009 (data available at http://www.nodc.noaa.gov/OC5/WOA09/pr_woa09.html).

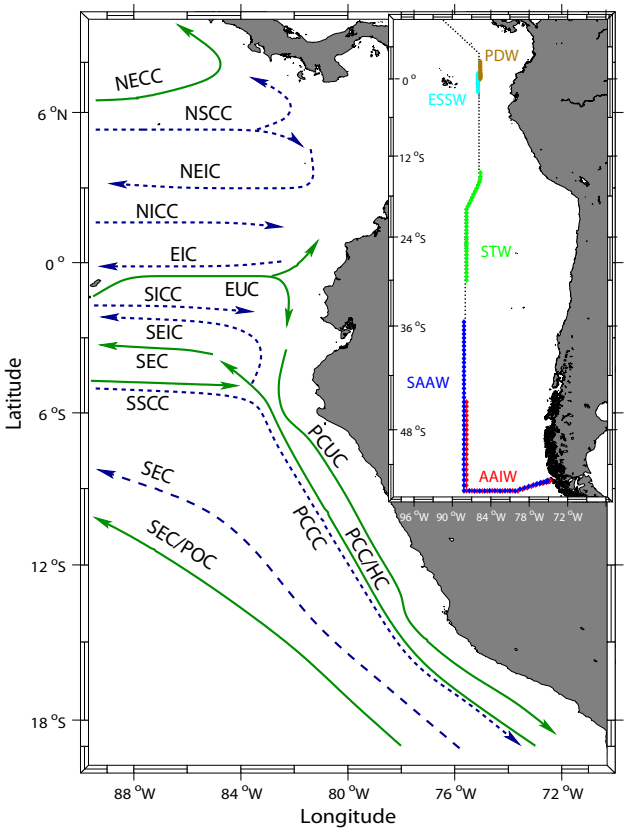

Fig. 1b. Circulation scheme for currents in the upper 200 m (green lines) and 200–600 m (blue dashed lines) layers based on descriptions provided by Kessler (2006), Czeschel et al. (2011) and Grasse et al. (2012); notice that some current bands may cover both depth layers. The current shown are: NECC – North Equatorial Counter Current, NSCC – Northern Subsurface Counter Current, NEIC – North Equatorial Intermediate Current, NICC – North Intermediate Counter Current, EIC – Equatorial Intermediate Current, EUC – Equatorial Undercurrent, SICC – South Intermediate Counter Current, SEIC – South Equatorial Intermediate Current, SSCC – Southern Subsurface Counter Current, SEC – South Equatorial Current, POC – Peru Oceanic Current, PCCC – Peru–Chile Counter Current, PCC/HC – Peru–Chile or Humboldt Current and PCUC – Peru–Chile Undercurrent. The inset shows the source regions (coloured) along the P19 cruise track, where the source water masses (Table 1) were defined.

In this paper we will use two occupations of a section along 85°50′ W, carried out in 1993 and 2009, to examine the temporal evolution of the OMZ in the tropical eastern South Pacific Ocean. The area of investigation extends from the northeastern rim of the South Pacific subtropical gyre to the southern part of the Panama Basin (from 14° S to 1° N) (Fig. 1a). It is a region poorly ventilated by the eastern part of the equatorial current system and by the northern part of the Peru–Chile current system, with relatively long residence times (Kessler, 2006). A schematic of the currents is shown in Fig. 1b. This region is influenced by El Niño/La Niña–Southern Oscillation (ENSO), one of the strongest modes of interannual variability in the global ocean/atmosphere system (e.g. Philander, 1983). El Niño and La Niña refer respectively to the warm and cold ocean phases of the near-surface waters in the central and eastern Pacific Ocean. During an El Niño event, the upwelling of nutrient-rich waters off the Peruvian coast is suppressed, with dramatic consequences for fisheries (Barber and Chavez, 1983).

The two occupations of the 85°50′ W transect represent contrasting ENSO phases. The 1993 cruise was completed during a weak warm event (the Oceanic Niño Index, ONI, was 0.5 for the February to March period) which was not catalogued as an El Niño because it lasted only four consecutive seasons, rather than the required five. The 2009 cruise was completed during a weak to moderate cold period (the ONI was −0.9 for December to February) which was not catalogued as a La Niña for the same reason (it lasted only four consecutive seasons). However, for the purposes of this study, we will consider the 1993 warm event as an

El Niño event, and the 2009 cold event as a La Niña event, because the magnitude and the sign of the ONI during both events qualify for this consideration, despite not lasting long enough to meet the duration criteria.

Superimposed onto the ENSO variability, the region is influenced by the Pacific decadal oscillation (PDO) which operates on time scales of several decades (Mantua et al., 1997; Chavez et al., 2003). The PDO also oscillates between warm (El Viejo) and cold (La Vieja) phases that go along with changes in sea surface height, sea surface temperature (SST), thermocline depth and ocean currents. Given their different time scales, ENSO has more impact on upper water masses, while the PDO can induce more substantial changes over the whole permanent thermocline and intermediate layers, e.g. influencing the dissolved oxygen content down to 700 m in the water column (Stramma et al., 2010a; Czeschel et al., 2011). A recent model study (Deutsch et al., 2011) showed that the PDO can modify the thermocline depth and thus trigger an upward migration of the OMZ during La Vieja phases. In the middle to late 1990s there was a shift to the cold phase (Chavez et al., 2003, 2008); therefore the 1993 cruise was completed by the end of an El Viejo, whereas the 2009 cruise took place under La Vieja conditions.

The eastern tropical Pacific OMZ is an important sink for oceanic-fixed nitrogen in the world ocean (e.g. Morales et al., 1999; Codispoti et al., 2001). The oceanic nitrogen can be removed in two ways. The first is via denitrification, i.e. the heterotrophic reduction of nitrate (NO_3^-) through several steps, with gaseous dinitrogen (N_2) as the final product. This process has been observed typically for waters with dissolved oxygen concentrations of less than 5 µmol kg^{-1}, although recent studies indicate that it remains active until higher concentrations (Codispoti et al., 2001; Kalvelage et al., 2011). The second is via the anammox process, i.e. the anaerobic oxidation of ammonium (NH_4^+) with nitrite (NO_2^-), which produces N_2 and water as the final products (Kuypers et al., 2005; Lam et al., 2009; Kalvelage et al., 2011). In the Peruvian OMZ, the nitrite produced during denitrification represents two thirds of the nitrite used for anammox (Lam et al., 2009). Recent studies point to anammox as the most important pathway for nitrogen removal within the OMZ (Kuypers et al., 2005; Thamdrup et al., 2006; Hamersley et al., 2007; Kalvelage et al., 2011).

Tsuchiya and Talley (1998) presented a comprehensive discussion about the structure of water masses along 85°50′ W. Basically, five different water masses were identified as contributing to the southeast Pacific Ocean. The top 200 m are occupied by subtropical water (STW) and subantarctic water (SAAW). Immediately below, and down to about 600 m, equatorial subsurface water (ESSW) is the predominant water mass. Coexisting with ESSW and reaching further deep, between about 500 and 1000 m, there is a significant contribution of antarctic intermediate water (AAIW). The deep layers, at depths greater than about 1100 m, are dominated by pacific deep water (PDW). In this study we will thoroughly characterise the properties of these water masses and use the extended optimum multiparameter (OMP) analysis to quantify the changes in water mass contributions and biogeochemical processes between the 1993 and 2009 occupations. In addition, we will analyse three zonal sections (along 3°35′, 6° and 14° S) carried out in 2009, running between the continental shelf region and 85°50′ W (Fig. 1a).

The OMP analysis (Tomczak and Large, 1989) has been used in the past to examine the distribution of water masses in the eastern South Pacific: off Chile (Silva et al., 2009), along the Chilean continental slope (Llanillo et al., 2012), and south of 10° S (De Pol-Holz et al., 2007). Here we will use the extended OMP analysis (Karstensen and Tomczak, 1998; Hupe and Karstensen, 2000), which decomposes the observed parameter distribution into contributions that originate from water mass mixing and those that stem from remineralization/respiration as well as denitrification processes. In this way it is possible to investigate the relative roles of both ocean transport (linked to the advection and mixing of water masses) and biogeochemical processes on the changes arising between the two cruises.

2 Data and methods

2.1 Observational data

Our study is based on two data sets taken in 1993 and 2009, respectively, which include both conductivity-temperature-pressure (CTD) and oxygen/nutrient (bottle) data. The P19 data set was acquired during the World Ocean Circulation Experiment (WOCE) aboard R/V *Knorr*, with full-depth stations from southern Chile to Guatemala. The section runs along 88° W in the South Pacific but shifts to 85°50′ W in the equatorial Pacific (Tsuchiya and Talley, 1998). The stations between 14° S and 1° N were carried out from 23 to 31 March 1993. About 16 yr later, from 27 January to 19 February 2009, the R/V *Meteor* cruise M77/4 (hereafter M77) reoccupied the WOCE P19 stations between 14° S and 1° N, with stations separated (on average) by about 60 km, although with improved resolution near the Equator (Fig. 1a). M77 focused on the OMZ waters, and therefore most of the stations reached down to only 1200 dbar. The two cruises covered the tropical region during approximately the same season (about 1.5 months' difference), so the seasonal differences are expected to be small as compared with the interannual and interdecadal changes. The sampling accuracy of the data from the M77 (P19) cruise was: < 0.001 (0.002) for salinity, 0.72 (1.34–1.78) µmol L^{-1} for oxygen, 0.278 (0.3–0.4) µmol L^{-1} for nitrate, 0.009 (0.02–0.03) µmol L^{-1} for phosphate and 0.18 (1–2) µmol L^{-1} for silicate, respectively.

Table 1. Source water types used for the extended OMP analysis. The source water masses are subtropical water (STW), subantarctic water (SAAW), equatorial subsurface water (ESSW), antarctic intermediate water (AAIW) and pacific deep water (PDW). The weights used for each parameter are included in the bottom row. The oxygen saturation concentrations based on the source water types of temperature and salinity are given in the last column (based on Garcia and Gordon, 1992).

Water mass	Pot. Temp. (°C)	Salinity	Oxygen (μmol kg^{-1})	Phosphate (μmol kg^{-1})	Silicate (μmol kg^{-1})	Nitrate (μmol kg^{-1})	Oxygen saturation
STW	20.8	35.52	240.65	0.46	2.23	0.74	221.55
SAAW	11	34.00	268.2	1.07	2.17	13.7	270.74
ESSW	10	34.80	13.6	2.43	29.81	32.7	275.00
AAIW	3.0	34	238.2	1.97	24.6	28.5	324.97
PDW	1.82	34.67	105.2	2.76	157.3	38.42	332.94
Weight	24	24	7	7	3.5	7	Mass cons. 24

The bottle data from both cruises and the results obtained with the OMP analysis (applied at each data point) have been objectively interpolated onto a regular grid with 25 m depth spacing and 60 km horizontal spacing, from just below the average mixed layer depth (55 m) down to 1200 m. An influence radius of 100 km in the horizontal and an increasing influence radius from 15 m at 55 m depth to 250 m at depths of 1200 m in the vertical were applied. A comparison (not shown) of temperature, salinity and oxygen data, available at both low (bottle) and high (CTD) vertical resolution, reveals that the interpolated bottle data reproduces the CTD data distribution well. Therefore, for this study we have used interpolated bottle data for all parameters.

2.2 Extended optimum multi-parameter (OMP) analysis

The extended OMP analysis (Hupe and Karstensen, 2000; Karstensen and Tomczak, 1998) evolved from the inverse modelling techniques described by Mackas et al. (1987) and Tomczak and Large (1989). The OMP analysis finds solutions, in the form of water mass fractions, to a set of linear mixing equations. In contrast to the classical mixing-triangle approach, which is based on temperature and salinity only, the OMP analysis utilizes more parameters (such as oxygen and inorganic nutrients) to determine the water mass fractions which are required to be non-negative. The extended analysis is based on a multidimensional least-square fit that allows resolving the mixing of more than three water masses, as well as the biogeochemical cycling (respiration, remineralization and denitrification signals).

The application of the OMP analysis requires a correct definition of the source water masses expected to contribute to the observed parameter field. To control the influence of a certain parameter on the solution, a weighting is applied (Table 1, last row). This weighting considers the environmental variability within the region of water mass formation and the overall span of the parameter space in the source water matrix (Tomczak and Large, 1989). Further details on the technique, such as the data normalization scheme and the parameter weighting criteria, can be found in Tomczak and Large (1989).

The standard OMP analysis assumes that all parameters are conservative quantities; that is, they are only modified by mixing. This is difficult to justify when biogeochemical processes, such as the remineralization of organic matter and denitrification, are likely to contribute to the observed parameter distribution. The extended OMP analysis (Hupe and Karstensen, 2000; Karstensen and Tomczak, 1998; Poole and Tomczak, 1999) solves this issue (the non-conservative behaviour of parameters) by adding stoichiometry-scaled remineralization/respiration (influencing oxygen, nitrate, phosphate and silicate) and denitrification (influencing nitrate and phosphate) processes to the set of linear equations. The solution technique follows that for the standard OMP: the system must be over-determined in order to ensure an unambiguous solution and to provide for error estimates. Given the available parameters in the M77/P19 data sets (potential temperature θ, salinity S, dissolved oxygen O_2, nitrate NO_3, phosphate PO_4 and silicate SiO_4), and assuming mass conservation (the sum of water mass fractions is one), the contribution of up to four source water masses and the transformations due to remineralization/respiration and denitrification can be resolved.

The extended OMP analysis is also based on the assumption that the source waters are time invariant. Hence, changes in the water mass fractions and the biogeochemical signals are interpreted as responding solely to the redistribution of water masses and to different biogeochemical cycling (remineralization, denitrification). To quantify the influence of temporal and natural variability on the results, we have run a series of sensitivity tests by simultaneously perturbing all water types with Gaussian noise in a series of Monte Carlo experiments (see Supplement). From these tests we conclude that the influence of temporal and natural variability is low and that the results obtained are robust.

The extended OMP analysis has been applied to the data of each transect, but excluding those data points located within the mixed layer, as they are influenced by air/sea interaction processes which are not considered in the set of equations, and which may introduce sources and/or sinks to the thermodynamic parameters (Holte et al., 2012).

2.3 Source water masses

To apply the OMP analysis to the P19 and M77 data, we first identify all possible contributing source water masses mainly based on the discussions by Tsuchiya and Talley (1998) and Fiedler and Talley (2006). Characterized by a subsurface salinity maximum (~ 35.5) (Wyrtki, 1967), the STW is formed to the southwest of the 85°50′ W transect by shallow subduction in a region where evaporation exceeds precipitation (Stramma et al., 1995). Shallow salinity minimum water (Reid, 1973; Tsuchiya and Talley, 1998; Karstensen, 2004) originates through the subduction of SAAW under STW, in the region between the subantarctic and subtropical fronts all along the southern rim of the South Pacific subtropical gyre. Not to be confused with the deeper (600–1100 m) salinity minimum of AAIW (~ 34), the SAAW is characterized by a salinity minimum of 34.0 and by temperatures about 11 °C, located between 100 and 200 m. The SAAW is advected north with the Peru–Chile (PCC) or Humboldt Current (HC) (Wyrtki, 1967) and partially ventilates the upper part of the OMZ (Fig. 1b).

Being a product of multiple and complex mixing in the equatorial region (Wyrtki, 1967), the ESSW is advected with relatively high oxygen content ($\sim 69.7\,\mu mol\,kg^{-1}$) into the OMZ region by the eastward equatorial current system, mainly by the Equatorial Undercurrent (EUC) (Stramma et al., 2010a). ESSW spreads southwards very slowly, almost stagnant, to the OMZ region, where its oxygen content decreases even further ($\sim 13.6\,\mu mol\,kg^{-1}$ in the P19 stations used as source region for ESSW, Fig. 1b). ESSW is slightly less salty (~ 34.8) and colder ($\sim 10\,°C$) than the overlying STW ($\sim 20.8\,°C$), and presents higher nutrient and lower oxygen concentrations than the STW. Part of the nutrient-rich ESSW contributes to the waters that upwell along the Peruvian coast (Brink et al., 1983).

The prominent salinity minimum that characterizes the AAIW is already eroded (~ 34.54) at this latitude range. This salinity minimum is located under both ESSW and SAAW, centred at depths between 600 and 1100 m. Formed by subduction between the subpolar and polar fronts (Hartin et al., 2011), the AAIW source water has high oxygen and low nutrient concentrations. Below the AAIW and centred at depths between 2500 and 3000 m, the PDW is characterized by a broad silicate maximum ($\sim 157.3\,\mu mol\,kg^{-1}$). PDW comes to this region following an intricate path through the North Pacific, and is believed to be the return flow of modified bottom waters originating in the South Pacific in the Antarctic Circumpolar Current (ACC) (Reid 1973; Tsuchiya and Talley, 1998). As we are concentrating our analysis on the upper 1200 m of the water column, other deep waters such as circumpolar deep water or antarctic bottom water are not considered here.

The initial step for defining the source water characteristics, summarized in Table 1, is to set the temperature/salinity source water values (water types) using information available in the literature (Tsuchiya and Talley, 1998; De Pol-Holz et al., 2007; Silva et al., 2009; Llanillo et al., 2012). Next, the data points within a range of temperature and salinity values, centred on the temperature/salinity water type definition for each water mass, are selected. Then, we impose geographical and depth constraints to pick only those data points that actually lay within the defined water mass formation areas. Finally, the selected data points are used to calculate the associated nutrient (NO_3, PO_4 and SiO_4) and oxygen source water types by averaging their respective values (Table 1).

The location where the formation areas are defined determines the initial water types, also influencing the OMP-derived mixing fractions and biogeochemical signals (the bulk of biogeochemical processes is derived in reference to the characteristics of the source water masses). As the focus of our study (and accordingly our interpretation) is on the regional changes in water-mass structure and remineralization/respiration/denitrification processes, we have defined all source water formation areas within the P19 cruise line track (Fig. 1b). We do not attempt to over-interpret the data, thus we avoid making statements on the full along-path transformation and biogeochemical cycling of all water masses. For this purpose we would need to define all source water masses in their original formation region at the surface.

To assess if these initial source water types are properly defined, we have investigated the stability of the OMP results through a series of Monte Carlo simulations, where random Gaussian noise is added to the parameters with the largest weights on the solution (temperature and salinity). This technique allows us to optimise the source water types as those that have the lowest residuals. The final water types are presented in Table 1.

The remineralization of organic matter and the associated respiration are included in the analysis via a set of Redfield ratios (Redfield et al., 1963), as they connect the changes in inorganic nutrients and oxygen. We use the Redfield ratios $-170 : 16 : 1$ corresponding to $\Delta O_2 : \Delta NO_3 : \Delta PO_4$ (Anderson and Sarmiento, 1994). The ratio $\Delta SiO_4 : \Delta PO_4$ is affected by the dissolution of opaline silica (Hupe and Karstensen, 2000) and shows regional variations depending on the plankton composition (Poole and Tomczak, 1999). Therefore, we use all available data to compute the best linear fit between silicate and phosphate for each cruise. The obtained values are $14.5 : 1$ for the M77 data set and $18.4 : 1$ for the P19 data set (see Supplement). However, we acknowledge that silicate shows different behaviour with depth, being remineralized deeper than the other

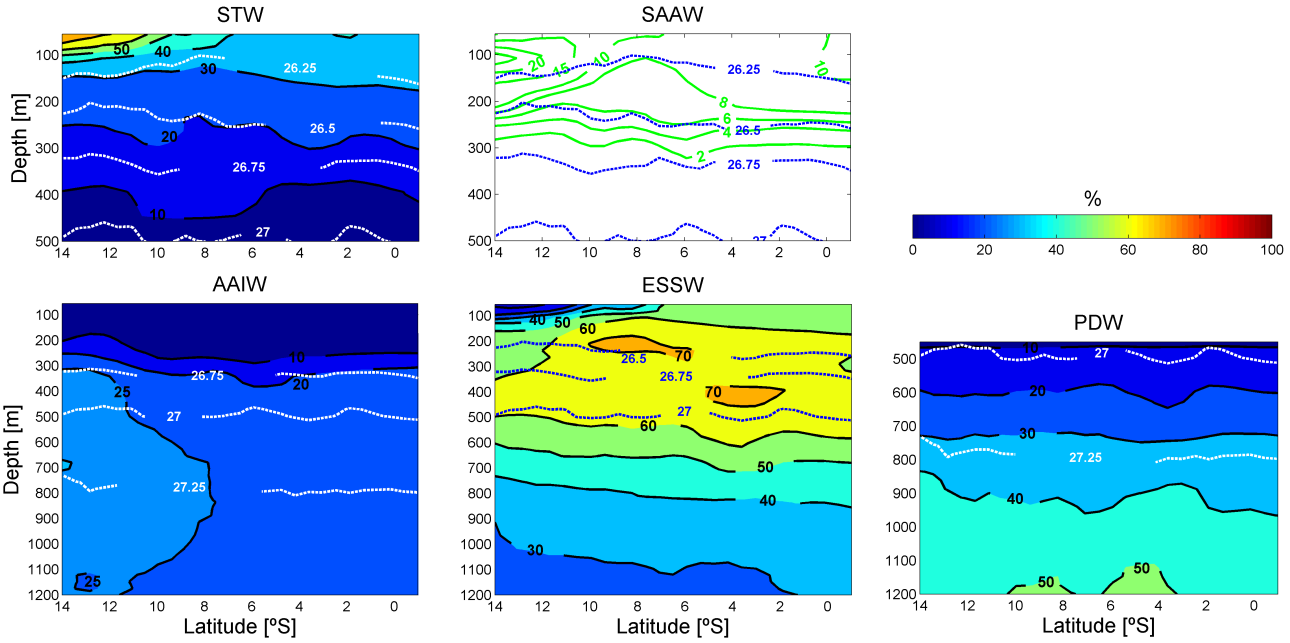

Fig. 2a. Water mass distribution (%) along the 85°50′ W section between 14° S and 1° N for the M77 cruise (February 2009), for subtropical water (STW), subantarctic water (SAAW), antarctic intermediate water (AAIW), equatorial subsurface water (ESSW) and pacific deep water (PDW) as defined in Table 1. Selected isopycnals are shown as dotted white/blue lines.

parameters bound in the organic matter. Therefore, silicate will show a non-constant ratio with phosphate and nitrate during remineralization/dissolution. Taking this into account, we assigned silicate the lowest weight (Table 1), so this parameter has only a weak influence on the solution.

Furthermore, the amount of PO_4 remineralized during denitrification is assumed to follow a ratio of $-1:0.01$ for $\Delta NO_3:\Delta PO_4$ (Gruber and Sarmiento, 1997). The extended OMP analysis only accounts for the first step of the denitrification process (the anaerobic reduction of NO_3 to NO_2). Whether this NO_2 is then used in the anammox process or follows the denitrification route, both ending in the loss of oceanic nitrate, cannot be elucidated with the current extended OMP analysis.

The OMP analysis is divided into two depth ranges (upper and lower) in order to limit the number of source water masses and to ensure an over-determined system of equations. We decided to break the OMP analysis at the 450 m depth horizon, because in this way the residuals are minimised in the upper part of the analysis (close to this cutting depth). Additionally, this cutting depth prevents the relatively higher residuals, characteristic of the upper part (0–4 %), from appearing in the lower part, which is characterized by much lower residuals. Finally, this partition leads to a smooth transition in the mixing fractions of ESSW and AAIW between the upper and lower part of the analysis. We run the upper analysis with STW, SAAW, ESSW and AAIW, and the lower analysis with ESSW, AAIW and PDW. To account for possible outliers in the data set, only those results from the OMP analysis which have mass conservation errors of less than ∼ 4 % are considered; following this condition, we discarded 0.5 % of the data points in the M77 section and 0.7 % of the data points in the P19 section.

3 Results

In this section we present the results derived from applying the extended OMP analysis to both the P19 and the M77 cruise data, specifically the contribution of the different water masses and the biogeochemical signals (respiration, denitrification) along the oceanographic sections. These quantities are useful descriptors of the regional physical and biogeochemical processes. In addition, the differences between the results obtained for both occupations (Sect. 4) provide information on the changes in time.

3.1 Water mass distribution

The water mass distribution for the recent M77 data, as obtained with the extended OMP analysis, illustrates the coexistence and mixing of water masses of equatorial, subtropical, subantarctic and antarctic origin along the 85°50′ W section, between 14° S and 1° N (Fig. 2a). The distribution obtained for the P19 data (Fig. 2b) along the same latitude range shows similar patterns to those found in the M77 data, and complements an earlier distribution obtained by applying the classic OMP analysis (De Pol-Holz et al., 2007) to the southern part of the P19 section

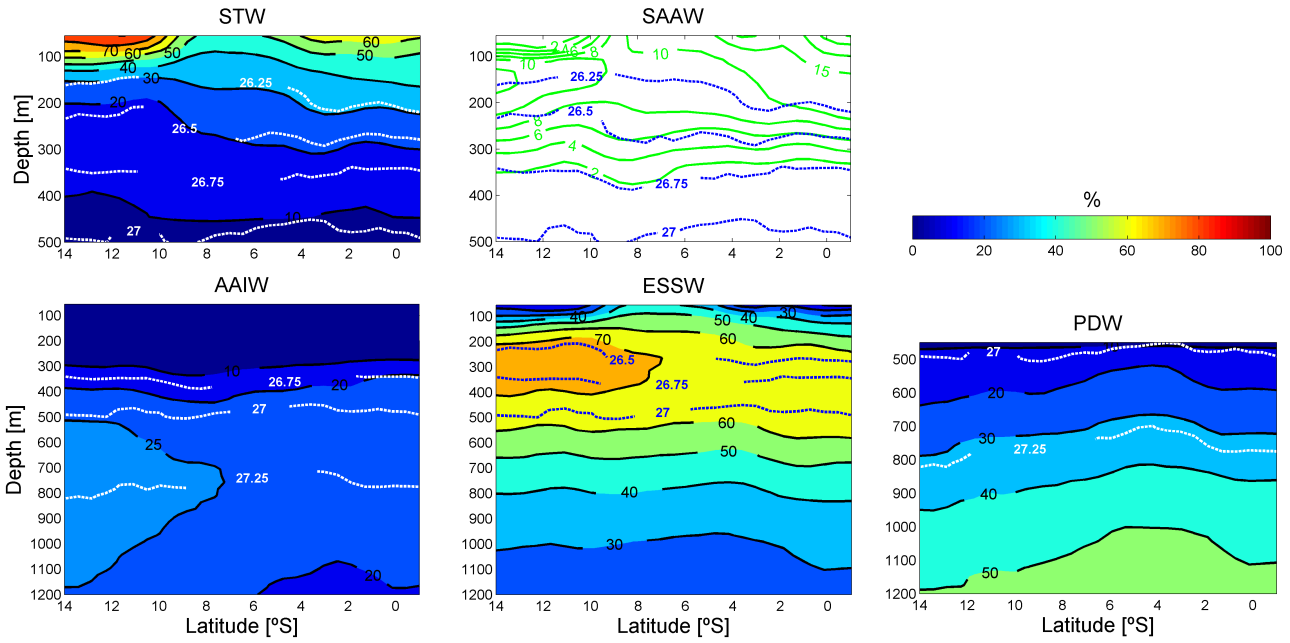

Fig. 2b. Water mass distribution (%) along the 85°50′ W section between 14° S and 1° N for the P19 cruise (March 1993), for subtropical water (STW), subantarctic water (SAAW), antarctic intermediate water (AAIW), equatorial subsurface water (ESSW) and pacific deep water (PDW) as defined in Table 1. Selected isopycnals are shown as dotted white/blue lines.

(50–10° S). The general patterns along the whole P19 section are already visible from individual parameter distributions (e.g. presented in Tsuchiya and Talley, 1998). In brief, the shallow layers are composed of subtropical (STW), subantarctic (SAAW) and equatorial (ESSW) water masses, while at intermediate depths there is a predominance of equatorial water (ESSW) that overlays the antarctic water (AAIW). For levels deeper than about 1100 m, the predominant water mass is PDW.

STW is best represented (> 50–60 %) in the top 100 m, between 14 and 10° S, closer to its source region. SAAW is also well distinguished south of 10° S, reaching up to 20 % in the uppermost layer and below STW, but is not significant (< 4 %) below 250–300 m. The ESSW core, with a mixing fraction of about 70 %, is located between 200 and 400 m. AAIW contributes more than 25 % at the southern boundary of the region, with its core located at 700 m. AAIW is slowly diluted to the north and replaced mainly by ESSW (Fig. 2a).

In the equatorial region (4° S to 1° N) there are remnants of low-salinity waters of equatorial origin down to 200 m. These waters most likely originated north of the Equator in the Panama Bight, where enhanced precipitation under the Intertropical Convergence Zone (ITCZ) creates low-salinity surface waters that are subsequently advected to the south, eventually crossing the Equator (Tsuchiya and Talley, 1998). However, this water mass was not considered in the OMP analysis, because the system of equations would no longer be over-determined. Furthermore, its inclusion would not add additional information, as the selected OMP configuration is already capable of recognizing the fresh fingerprint of these equatorial waters, associating them with the likewise relatively fresh SAAW, which is almost totally eroded north of 10° S. Therefore, the observed presence of SAAW north of 4° S is to be associated instead with the presence of these equatorial fresh waters.

The distribution of water masses between 85°50′ W and the continental shelf was also deduced along three zonal sections carried out during the M77 cruise (2009) at 14°, 6° and 3°35′ S (Figs. 3–5). SAAW has the highest percentage (> 20 %) in the western part of the 14° S transect (Fig. 3), but is generally under 8 % at 6° S (Fig. 4) and increases again in the surface layers to about 10 % at 3°35′ S (Fig. 5). This increase is very likely an artefact caused by the presence of low-salinity equatorial surface waters as discussed above, and as also proposed by Tsuchiya and Talley (1998). AAIW participation reaches 30 % centred at 700 m along the whole transect at 14° S (Fig. 3), and decreases towards the Equator, with maximal contributions of 20 % at 3°35′S (Fig. 5). The observed decrease in the mixing fractions of both AAIW and SAAW north of 14° S agrees well with their northward path along the subtropical gyre.

The contribution of STW decreases rapidly as we move from the southern to the central and northern sections. This confirms the progressive recirculation of this water mass towards the ocean interior, south of the equatorial front, and back poleward along the boundary, as a result of advection by the Peru–Chile Counter Current (PCCC) (Strub et al.,

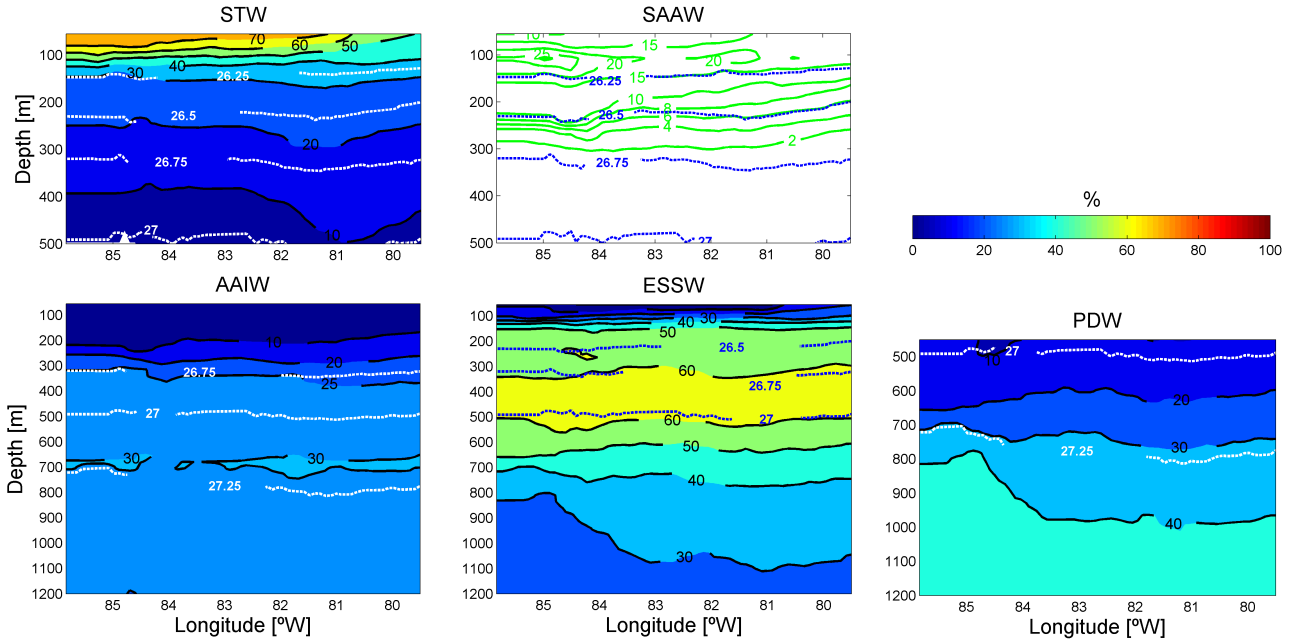

Fig. 3. Water mass distribution (%) along the 14° S section between 85°50′ W and the continental shelf for the M77 cruise (February 2009), for subtropical water (STW), subantarctic water (SAAW), antarctic intermediate water (AAIW), equatorial subsurface water (ESSW) and pacific deep water (PDW) as defined in Table 1. Selected isopycnals are shown as dotted white/blue lines.

1998). This can be appreciated at the offshore end of the 14° S section (Fig. 3).

ESSW is the predominant water mass in the 150–500 m depth range (50–60 %) for all zonal transects, with its core (70 %) located near 400 m; this core is most developed at 3° S (Fig. 3), where it spans the whole longitudinal transect. PDW becomes dominant (50 %) only in the deepest levels ($\geq$ 1100 m) of the section at 6° S.

3.2 Respiration and denitrification

The extended OMP analysis provides a bulk estimate of nutrient enrichment through the remineralization of organic matter, and oxygen depletion through the accompanying respiration, assuming a Redfield stoichiometry. As some of the water masses used in the analysis are created by complex mixing processes rather than by air/sea interaction processes, the respective source water types do not always reflect surface ocean concentrations. This is most obvious in the oxygen concentrations of the source water types that are, except for STW and SAAW, far from saturation (Table 1, last column). As such, the amount of respired oxygen (Figs. 6a, b) is to be seen relative to the source water type definitions. This is most prominent in the core of the OMZ, where one would expect to find the amount of respired oxygen to be larger than 200 µmol kg^{-1} (if all contributing water masses were defined at the surface), although the method determines only 30–50 µmol kg^{-1}. However, this is not a problem, as the focus of our study (and accordingly our interpretation) was on regional remineralization/respiration/denitrification, and thus we do not attempt to over-interpret the data. Nevertheless, it is clear that the OMZ is ventilated by water that is already rather low in oxygen concentrations, so that even moderate respiration can maintain the existence of the OMZ (Karstensen et al., 2008).

The patterns of remineralized nitrate and phosphate (phosphate not shown) closely follow the respired oxygen, with an inverse relation given by the Redfield ratios. Major deviations arise from the nitrate removal (and proportional phosphate enrichment, not shown) due to denitrification, also considered in the extended OMP analysis (Figs. 6a, b). The denitrified nitrate estimated from the OMP analysis is different from the directly observed nitrite. The extended OMP analysis is able to detect the signature of denitrification that took place outside the studied region and was advected into this area. In general our method has similarities with the quasi-conservative tracer approach (N^*) developed by Gruber and Sarmiento (1997), but also considers the mixing of water masses when estimating the denitrification. For both cruises the largest signal for nitrate removal via denitrification is found between 10 and 14° S, at a depth of about 200 m ($\sigma_\theta < 26.5$) (Fig. 6a), in agreement with previous studies (Lipschultz et al., 1990). However, this core of denitrification is probably linked to the advection of waters from the Peruvian shelf, where we assume this nitrate deficit originated (Fig. 6b). This advection of shelf waters seems to have increased during 2009 (M77 cruise, Fig. 6a), in good agreement with the expected reinforced

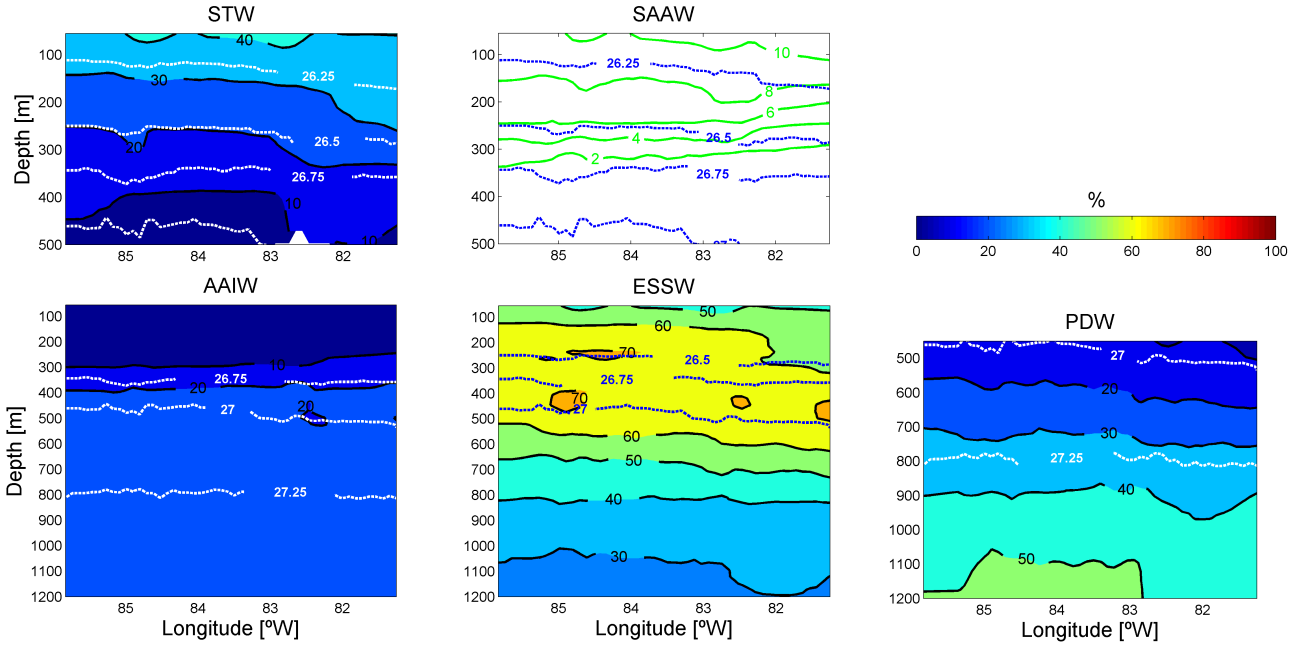

Fig. 4. Water mass distribution (%) along the 6° S section between 85°50′ W and the continental shelf for the M77 cruise (February 2009), for subtropical water (STW), subantarctic water (SAAW), antarctic intermediate water (AAIW), equatorial subsurface water (ESSW) and pacific deep water (PDW) as defined in Table 1. Selected isopycnals are shown as dotted white/blue lines.

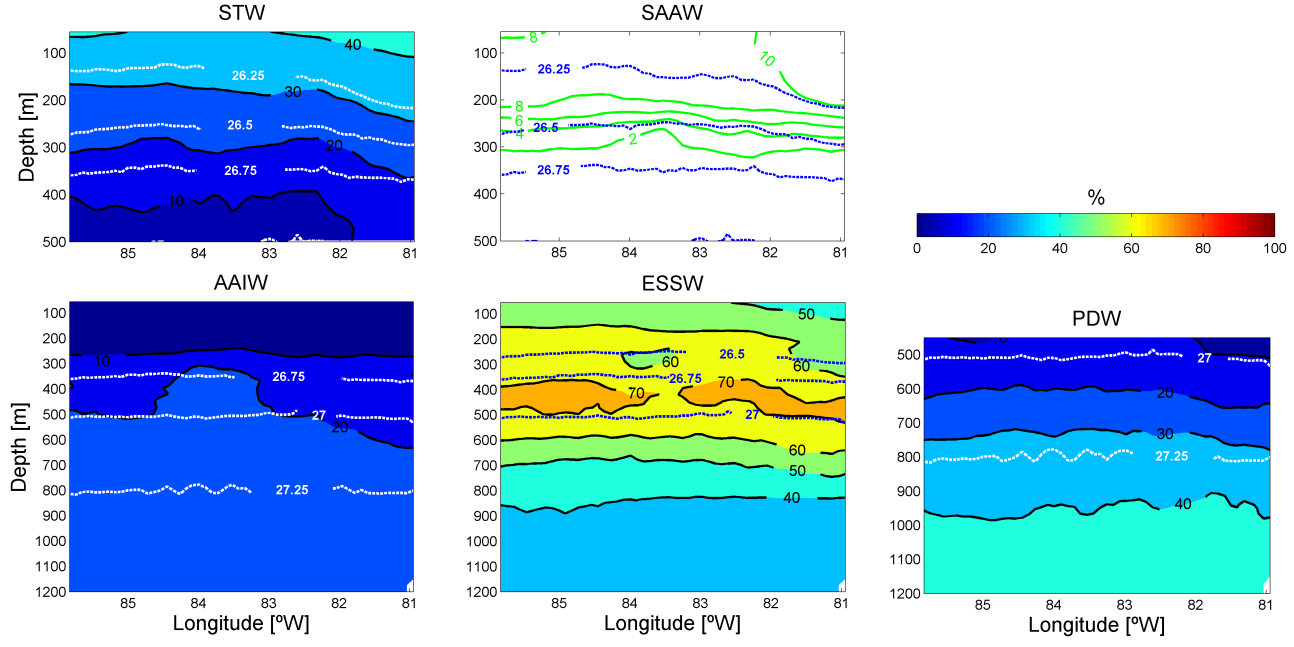

Fig. 5. Water mass distribution (%) along the 3°35′ S section between 85°50′ W and the continental shelf for the M77 cruise (February 2009), for subtropical water (STW), subantarctic water (SAAW), antarctic intermediate water (AAIW), equatorial subsurface water (ESSW) and pacific deep water (PDW) as defined in Table 1. Selected isopycnals are shown as dotted white/blue lines.

Ekman transport due to stronger trade winds during La Niña conditions. This near-surface denitrification core represents an important source of nitrite for the anammox process, as confirmed by previous studies which found the highest rates of anammox in the upper part of the OMZ off Peru/Chile (Hamersley et al., 2007; Thamdrup et al., 2006). A second core with denitrification signals is found for both cruises between 2 to 4° S and 10° S in the depth range from 350 to

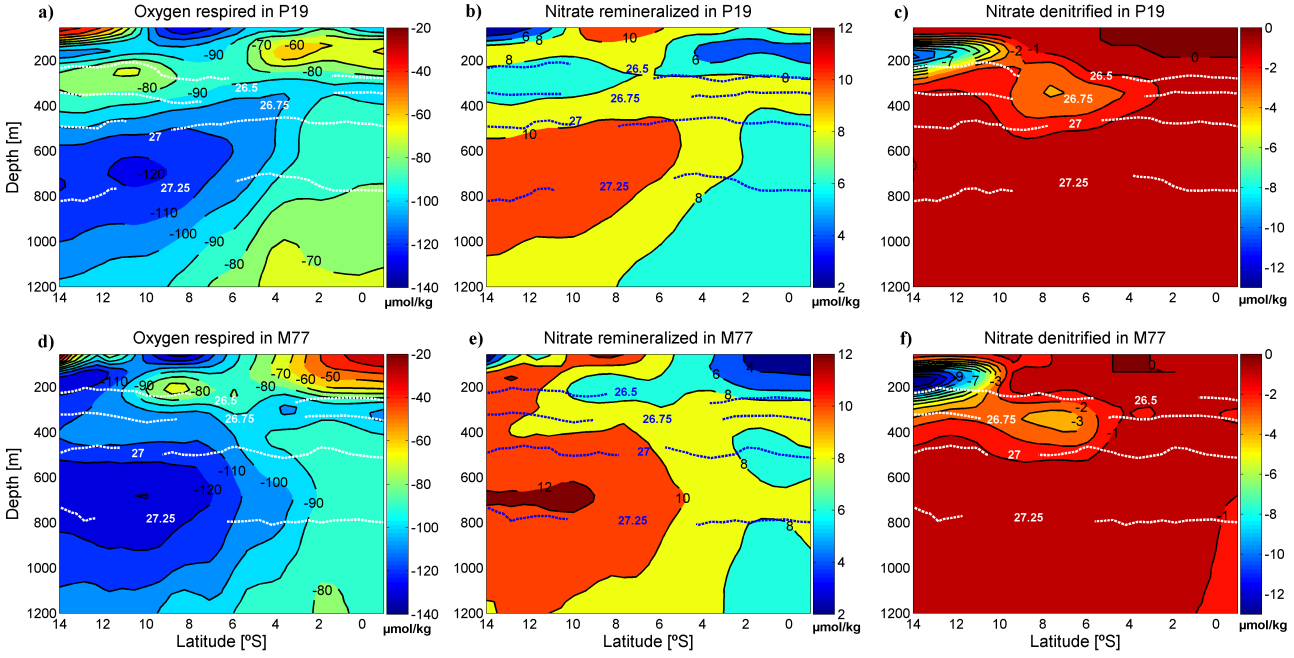

Fig. 6a. OMP-derived biogeochemical activity within the water column for the P19 (March 1993) and M77 (February 2009) cruises: **(a)** oxygen respired (µmol kg^{-1}) in P19, **(b)** nitrate remineralized (µmol kg^{-1}) in P19, **(c)** nitrate denitrified (µmol kg^{-1}) in P19, **(d)** oxygen respired (µmol kg^{-1}) in M77, **(e)** nitrate remineralized (µmol kg^{-1}) in M77, **(f)** nitrate denitrified (µ mol kg^{-1}) in M77. Selected isopycnals are shown as dotted white/blue lines.

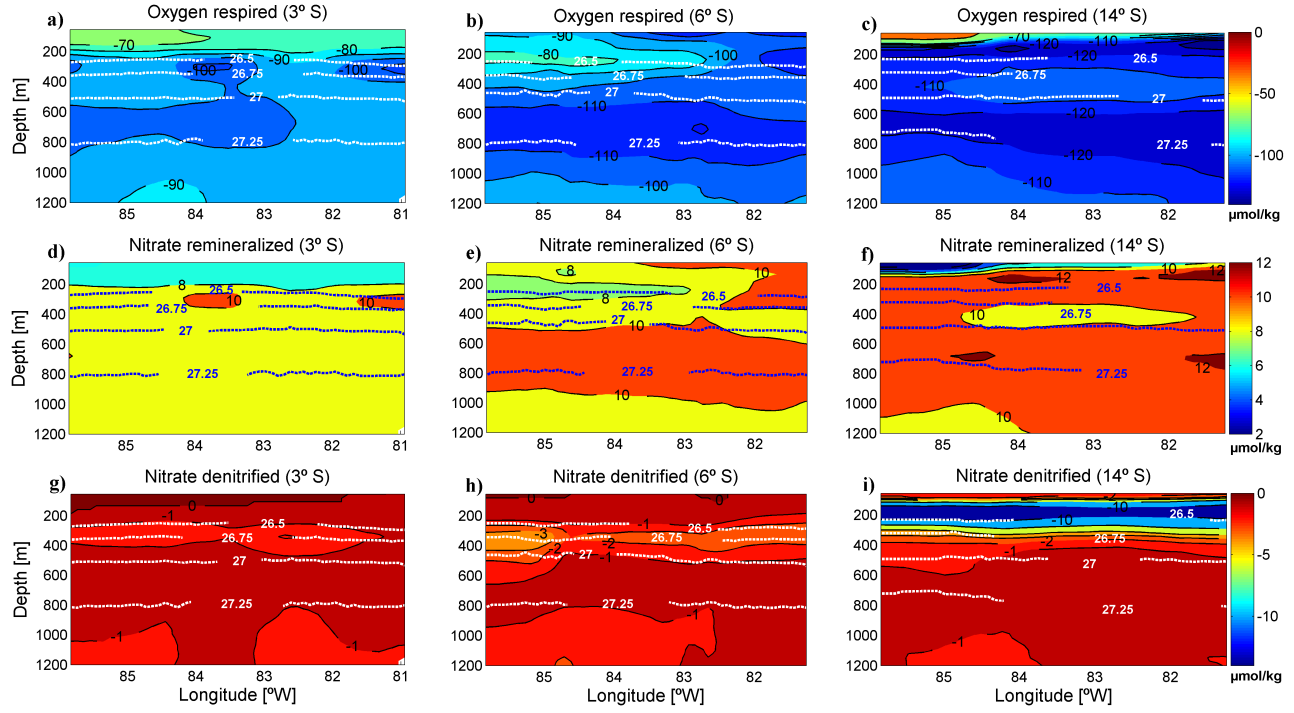

Fig. 6b. OMP-derived biogeochemical activity within the water column for the three zonal sections (3°, 6° and 14° S) completed during the M77 cruise (February 2009): **(a)** oxygen respired (µmol kg^{-1}) at 3° S, **(b)** oxygen respired (µmol kg^{-1}) at 6° S, **(c)** oxygen respired (µmol kg^{-1}) at 14° S, **(d)** nitrate remineralized (µmol kg^{-1}) at 3° S, **(e)** nitrate remineralized (µmol kg^{-1}) at 6° S, **(f)** nitrate remineralized (µmol kg^{-1}) at 14° S, **(g)** nitrate denitrified (µmol kg^{-1}) at 3° S, **(h)** nitrate denitrified (µmol kg^{-1}) at 6° S, **(i)** nitrate denitrified (µmol kg^{-1}) at 14° S. Selected isopycnals are shown as dotted white/blue lines.

500 m (about $26.5 < \sigma_\theta < 27$) and in agreement with earlier interpretations (Tsuchiya and Talley, 1998).

4 Changes along 85°50′ W between 1993 and 2009

Temporal changes in the spatial distribution of relevant biogeochemical parameters such as oxygen or nitrate may be caused by shifts in the water mass distribution (this includes changes in the advection, diffusion and isopycnal heave) and/or by changes in the biogeochemical activity (respiration and denitrification). Isopycnal heave may take place at very different temporal scales, from minutes (internal waves) and days/weeks (mesoscale phenomena) to interannual or interdecadal processes such as ENSO and PDO. In addition, there may be changes related to variations in the advection and mixing of the different water masses (e.g. Roemmich et al., 2007), the swifter the arrival of some specific water mass the greater its contribution and its influence on the local properties. Changes related to the variability of source water types, due to changes in air/sea interaction in the water mass formation at the source region (Bindoff and McDougall, 1994), cannot be directly considered by the OMP analysis although they may be reflected by changes in the water mass distribution.

Our aim here is to distinguish between the physical and biogeochemical components of the observed changes in oxygen and nitrate. The M77 versus P19 changes, either in the measured biogeochemical parameters or in OMP-derived water mass distribution and biogeochemical activity, are calculated by subtracting the 1993 value from the 2009 value at each gridpoint (M77–P19).

4.1 Measured changes in oxygen and nitrate content

The meridional sections of measured nitrate and dissolved oxygen during the P19 and M77 cruises are shown in Fig. 7, and their changes in time are depicted in Fig. 8. In the top few hundred metres (Fig. 8) there are a few locations possibly influenced by the surface and near-surface zonal currents. First, there is a decrease in dissolved oxygen (between -10 and $-20\,\mu mol\,kg^{-1}$) and an increase in nitrate (between 1 and $4\,\mu mol\,kg^{-1}$) in the 55–250 m depth range at the equator (Fig. 8). This corresponds to the location of the relatively oxygen-rich and nutrient-poor eastward flowing EUC. The weakening of the EUC (Czeschel et al., 2012) may explain the decrease in oxygen (and the increase in nitrate) found at this location, although it is not possible to discern how much of this weakening is caused by the seasonal variability (Johnson et al., 2002) and how much is due to La Niña conditions found in 2009. Second, there are two cores with oxygen increase at 8° S, a shallow one centred at 50 m with an increase between 10 and $25\,\mu mol\,kg^{-1}$, and a deep one centred at 225 m with an increase of $10\,\mu mol\,kg^{-1}$ (Fig. 8a). These cores may possibly be associated with the oxygen-rich eastward flowing Southern Subsurface Counter Current (SSCC) (Czeschel et al., 2011); however, both cores must have different origins, as the shallow core displays a reduction in the nitrate content, whereas the nitrate concentration of the deep core has increased (Fig. 8b). Third, between 11° and 9.5° S and in the 50–150 m depth range, we observe a core that has undergone an increase in nitrate (between 4 and $10\,\mu mol\,kg^{-1}$) and a decrease in oxygen (between -20 and $-50\,\mu mol\,kg^{-1}$) (Fig. 8). The same behaviour is found in another core located in the upper 250 m at 4° S. We identify the former core with the westward flowing South Equatorial Current (SEC) and the core at 4° S with the southern equatorial branch of the SEC (Czeschel et al., 2011). It is possible that wind-driven changes in the SEC (with stronger south-easterlies during the 2009 La Niña) may have caused the variations observed in oxygen and nitrate by strengthening these currents.

At 1° N and between 400 and 600 m, there is a core with nitrate decrease ($-1\,\mu mol\,kg^{-1}$) and slight oxygen increase ($5\,\mu mol\,kg^{-1}$) (Fig. 8), possibly associated with an increase in the transport of the eastward flowing North Intermediate Counter Current (NICC) (Czeschel et al., 2011). Between 3° and 5° S and in the depth range from 500 to 1000 m, we find oxygen depletion (between -5 and $-10\,\mu mol\,kg^{-1}$) and nitrate increase (between 1 and $2\,\mu mol\,kg^{-1}$, down to 1200 m) (Fig. 8). These changes may be related to a decrease in the westward flowing South Equatorial Intermediate Current (SEIC) (Czeschel et al., 2012), therefore enhancing the presence of ESSW at this location (Fig. 9).

4.2 Changes in water mass distribution

In the near surface layers (between 55 and 200 m) south of 10° S, there is a substantial increase in SAAW at the expense of STW (Fig. 9a). The apparent decrease in SAAW in the northern end of this section actually represents a decrease in the equatorial surface waters found south of the equator during the 2009 La Niña conditions (see Sect. 3.1). The increase in precipitation in the eastern equatorial Pacific during El Niño conditions could explain the larger content of equatorial surface water found in the 1993 data.

In the upper thermocline and upper intermediate waters, the dominant spatial trend is caused by two different phenomena: First, the upwelling/downwelling of ESSW associated with La Niña/El Niño conditions, respectively. Second, during 2009, the core of AAIW appears to flow along shallower isopycnals (Figs. 9b, 2a and b).

The ESSW decreases in the water column (south of 8° S) between 150 and 600 m, partially replaced by STW which increases between 200 and 300 m (from 8 to 2° S), and largely replaced by the upper part of AAIW (Fig. 9a). The upward expansion of AAIW also reaches down to its core (25 % contribution), centred around 700 m (Fig. 2a, b).

In order to discern which changes are due to the isopycnal heave associated with ENSO and which might be due to

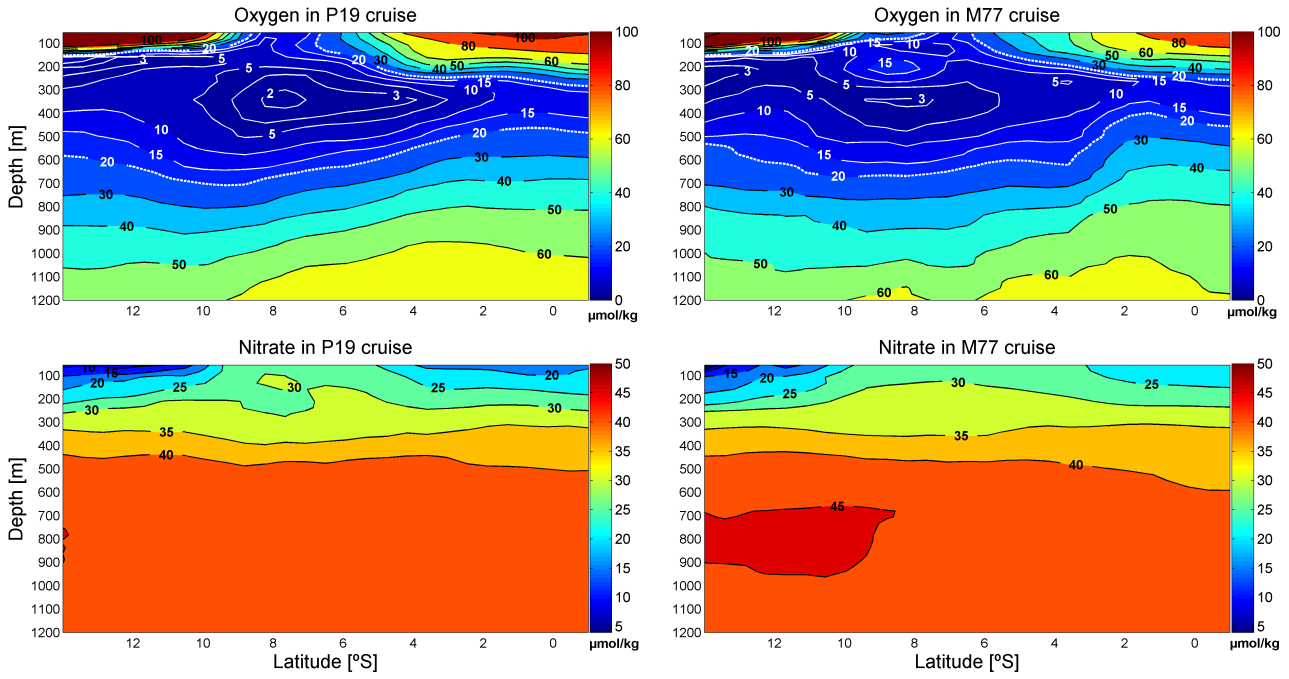

Fig. 7. Meridional section with measured oxygen (µmol kg^{-1}) and nitrate (µmol kg^{-1}) for the P19 (March 1993) and the M77 (February 2009) cruises.

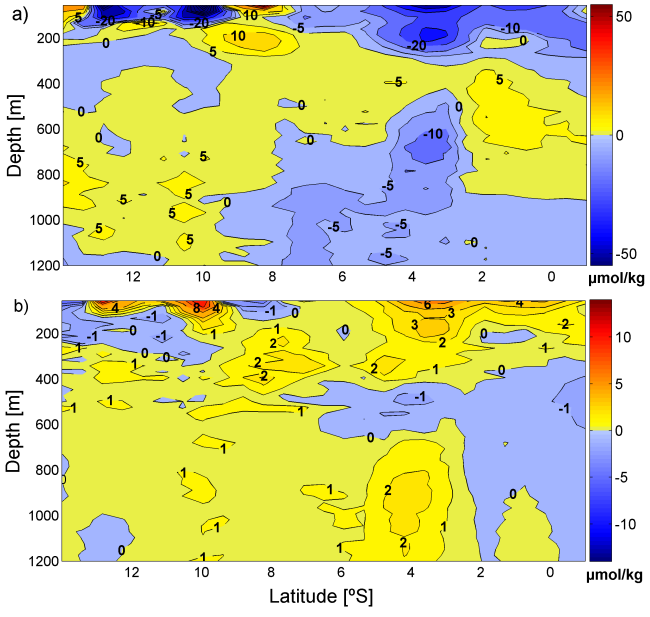

Fig. 8. Measured **(a)** oxygen (µmol kg^{-1}) and **(b)** nitrate (µmol kg^{-1}) changes between March 1993 and February 2009 (M77–P19).

other causes, we have repeated the analysis in density space. In Fig. 9b we can still appreciate the tongue of increasing AAIW (Fig. 9a) flowing along shallower isopycnals, which is in good agreement with the trends of warming and density reductions of the core of AAIW found by Schmidtko and Johnson (2012) in the eastern South Pacific. This tongue of shallower AAIW replaces ESSW and then advects more oxygenated waters into a different OMZ depth range (between 150 and 500 m) as it flows northward.

In the lower intermediate waters (450–800 m) there is an alternation in the predominance of ESSW and PDW, with a greater presence of PDW/ESSW at latitudes south/north of 8° S during the M77 cruise in 2009. The increase in ESSW appears centred between 5° and 3° S, at the location of the westward flowing SEIC (Czeschel et al., 2012). The enhanced presence of PDW south of 8° S (Fig. 9a) does not appear to be directly linked to the ENSO phenomenon; rather it may reflect the decadal shift of phase in the PDO from the 1993 warm El Viejo to the 2009 relatively cold La Vieja. However, the mixing fraction of PDW does not increase along the whole section (800–1200 m depth range) as expected during the La Vieja phase, perhaps related to a weakening of the SEIC. Nevertheless, the sensitivity tests grant us confidence in the robustness of this result (see Supplement). Further discussion remains beyond the scope of this paper.

4.3 Physical and biogeochemical contributions to oxygen and nitrate changes

By means of the extended OMP analysis, we may assess how much of the observed changes are related to variations in the water mass distribution (physical component which includes

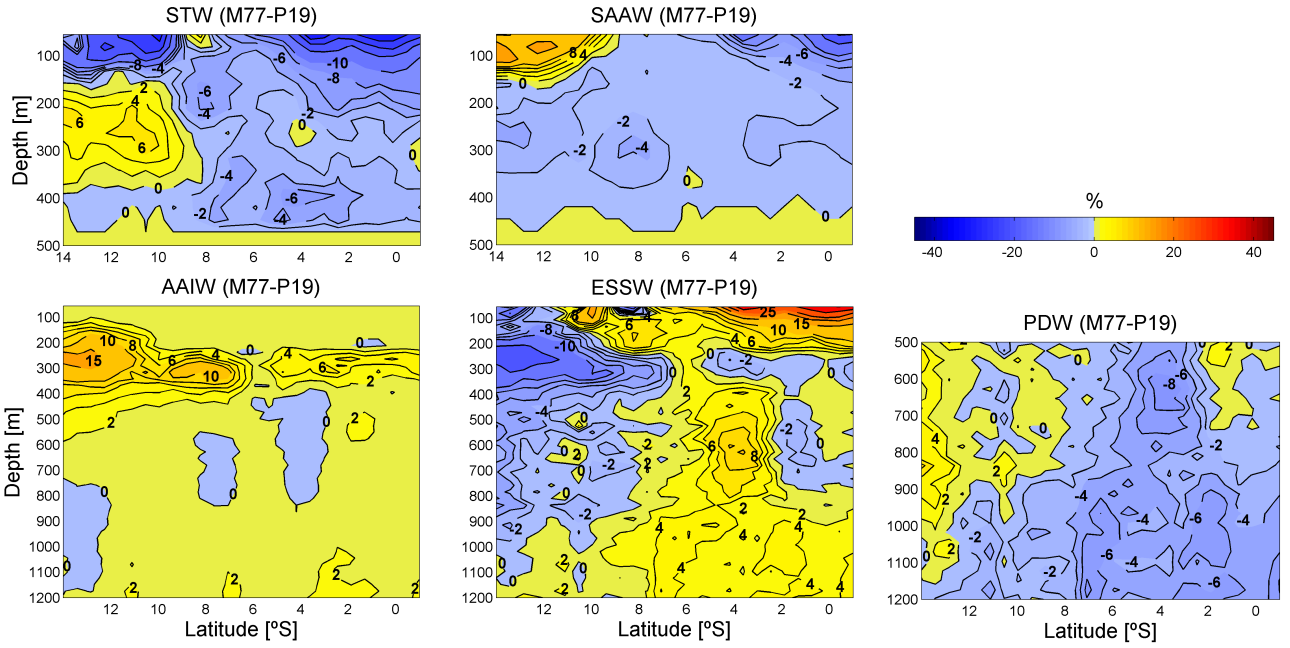

Fig. 9a. Water mass changes (%) between March 1993 and February 2009 (M77–P19) for subtropical water (STW), subantarctic water (SAAW), antarctic intermediate water (AAIW), equatorial subsurface water (ESSW) and pacific deep water (PDW).

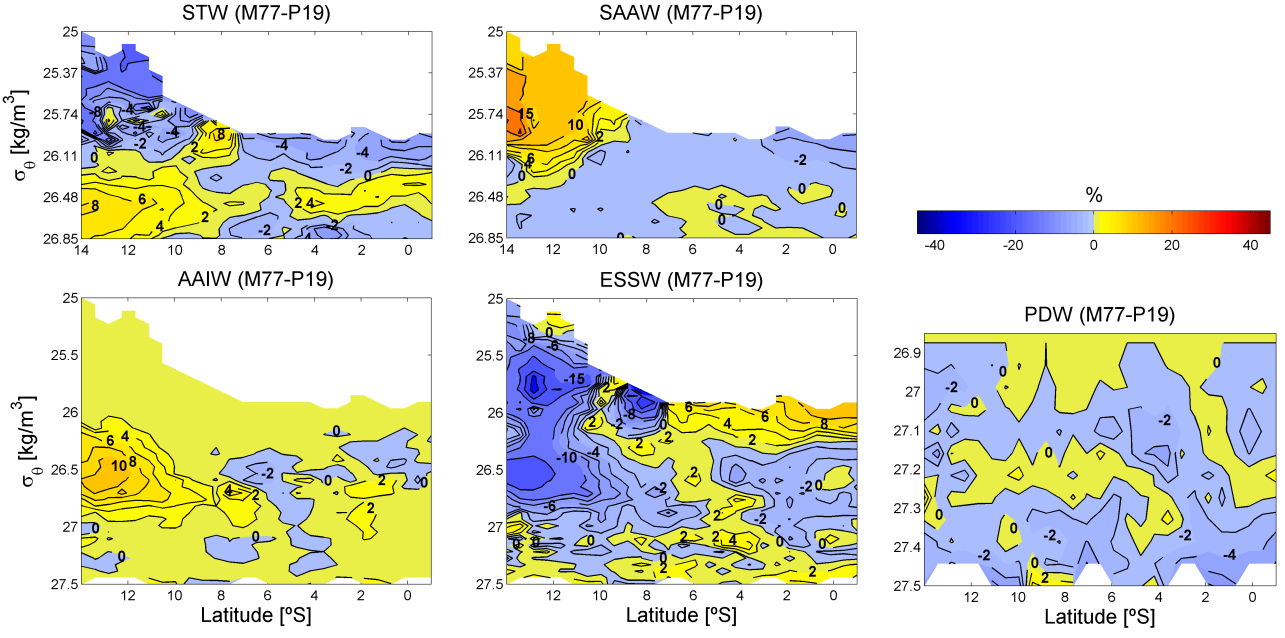

Fig. 9b. Water mass changes (%) in density space between March 1993 and February 2009 (M77–P19) for subtropical water (STW), subantarctic water (SAAW), antarctic intermediate water (AAIW), equatorial subsurface water (ESSW) and pacific deep water (PDW).

advection, diffusion and isopycnal heave) and how much is caused by changes in the respiration and denitrification signals (biogeochemical component). These biogeochemical changes should not be interpreted as variations in the biogeochemical rates, as calculating a rate requires knowing not only the characteristics of water masses at origin, but also an estimate of their age as they reach the studied area. Hereafter, we will refer to the physical component of change as "physical transport".

As each parameter (oxygen, nitrate) is bound to a residual (difference between the measured data and the OMP-modelled data), the exact contribution of each component of

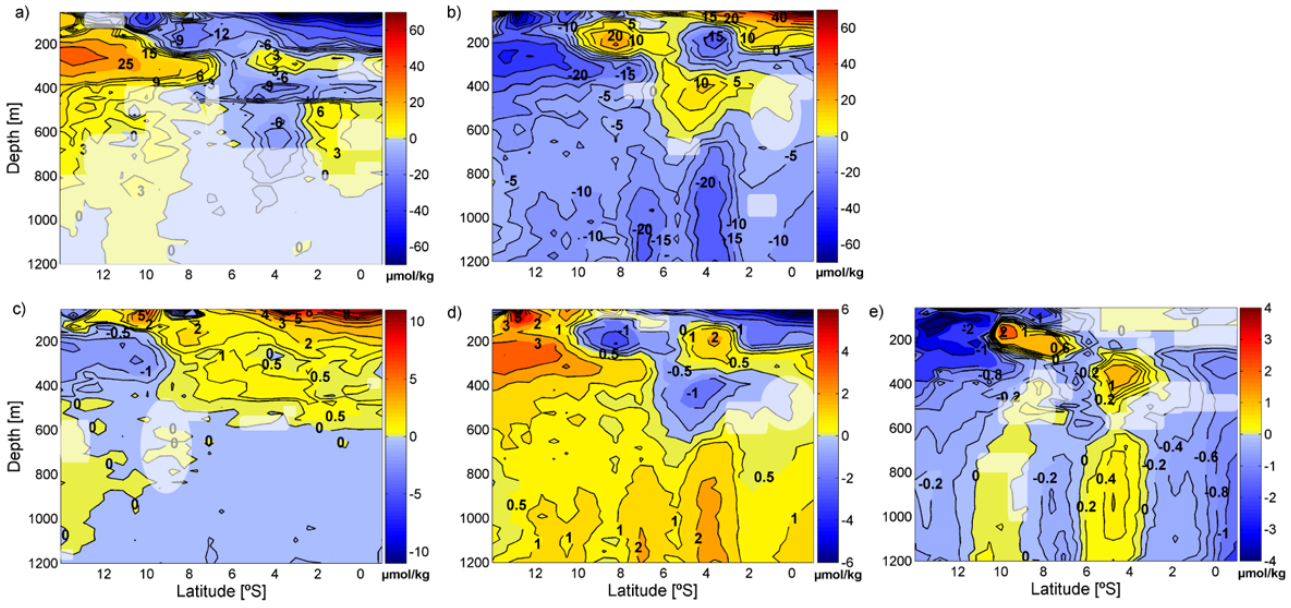

Fig. 10. OMP-derived changes in: **(a)** physical transport of oxygen (µmol kg^{-1}), **(b)** oxygen respired (µmol kg^{-1}), **(c)** physical transport of nitrate (µmol kg^{-1}), **(d)** remineralized nitrate (µmol kg^{-1}) and **(e)** denitrified nitrate (µmol kg^{-1}). White shading represents areas where the difference between the measured change and the OMP-modelled change is larger than either component of the change (physical or biogeochemical).

the change remains unknown, but we may still find out the significance of the physical and biogeochemical components.

The physical and biogeochemical contributions to the oxygen and nitrate changes between both cruises are shown in Fig. 10. The same analysis was done in density space with similar results (see Supplement). The white-shaded areas represent the points where the total error, or difference between the measured parameter change and the OMP-modelled parameter change (physical plus biogeochemical), is larger than either modelled component of change, i.e. outside the white-shaded areas the signal is larger than the noise, so the information provided is significant. Notice that this is the most restrictive scenario, as we are assuming that all the errors in the OMP fit are associated with only one component of the modelled change.

Within the OMZ waters, an increase/decrease of oxygen due to larger physical transport will naturally lead to more/less oxygen availability and increased/decreased respiration and nutrient remineralization. South of 6° S, a significant increase in the physical transport of oxygen is observed between 150 and 400 m (Fig. 10a), in good agreement with the previously proposed upward shift in the OMZ depth range ventilated by AAIW. This gain in oxygen is partially compensated by an increase in the respiration signal as more oxygen becomes available in this depth range of the OMZ (reflected in Fig. 10b as an apparent oxygen loss). The outcome is a net change in oxygen of smaller amplitude (Fig. 8a). In the upper 150–200 m (north of 8° S) this situation is reversed, as there is a general decrease in the physical transport of oxygen (Fig. 10a), an increase in the physical transport of nitrate (Fig. 10c) which is accompanied by a reduction in the oxygen available for respiration (reflected in Fig. 10b as an apparent oxygen gain) and, consequently, a reduction in the nitrate remineralized in the same locations (Fig. 10d). These results agree with a previous interpretation that pointed to an "oxygen-driven" remineralization intensity within the Chilean OMZ (Paulmier et al., 2006). These changes may be explained by the shift from the 1993 El Niño to the 2009 La Niña conditions, which promoted an upward displacement of the oxygen-poor and nutrient-rich ESSW.

The amount of nitrate loss due to denitrification is directly influenced by changes in oxygen availability, which ultimately depends on the interplay between oxygen supply and respiration. As also shown by our data, an increase in dissolved oxygen in the upper part of the water column takes place during El Niño conditions (Guillén et al., 1988), accompanied by a deepening of the upper part of the OMZ which dampens denitrification in the upper layers (Morales et al., 1999). During La Niña events the situation reverses: the reinforced upwelling promotes the rise in depth of the upper part of the OMZ, enhancing denitrification in the upper part of the water column (Morales et al., 1999). Therefore, the change of ENSO phase between both cruises may explain the increased nitrate loss observed between 1993 and 2009 in the upper 200 m south of 10° S (Figs. 6a, b and 10e). This increased signal of denitrification is most likely the result of

increased advection of waters from the Peruvian shelf, where denitrification occurred during La Niña conditions (Fig. 6b).

Further deep, between 250 and 500 m, the decrease in the volume delimited by the 1 µmol kg^{-1} nitrate loss isoline in 2009 (Fig. 6a) represents a decrease in the denitrification signal, and is corresponded by a core with apparent nitrate gain located between 11° and 7° S in the 100–300 m depth range (Fig. 10e). However, inside the core of this volume we find a more intense denitrification signal (~ 3 µmol kg^{-1}) in 2009 (Fig. 6a), associated with a slightly larger nitrate loss between 300 and 400 m from 8° to 6° S (Fig. 10e).

A decrease in the denitrification signal (and consequently an apparent nitrate gain) was also observed roughly between 11° and 8° S and between 6° and 4° S, from 600 to 1200 m (Fig. 10e). In contrast, below 600 m and away from these latitudinal bands, there was slightly more nitrate loss in 2009, located mainly north of 3° S and south of 11° S (Fig. 10e).

Changes in the intensity of the zonal currents of the equatorial current system, already discussed in Sect. 4.1, may also be appreciated at their specific locations when distinguishing between physical and biogeochemical forcings. In general, an increase in the intensity of an eastward flowing current (or a weakening of a westward flowing current) will show up as a gain in physically supplied oxygen, larger respiration and a decrease in the nitrate loss by denitrification (or a decrease in the denitrification signal). The situation is the opposite with a weakening of an eastward flowing (or a strengthening of a westward flowing) current.

5 Conclusions

In this paper we have examined the changes in the water mass structure and biogeochemical signals of two opposite phases of ENSO in the eastern tropical South Pacific. The observed changes in the upper 200 m north of 10° S are clearly influenced by the ENSO phenomenon. During the 1993 El Niño event, there was increased advection of relatively well-oxygenated STW from the west of the equatorial Pacific Basin which replaced the low-oxygen ESSW in the top 250 m of the water column. This input deepened the upper part of the OMZ, dampening denitrification in the upper layers. In addition, the northward advance of the shallow salinity minimum originated by subducted SAAW was reduced. In contrast, during the 2009 La Niña conditions, the reinforced trade winds drove enhanced upwelling, raising the upper part of the OMZ. The nutrient-rich and oxygen-poor ESSW replaced STW in the upper layers north of 10° S, inducing a reduction in the amount of oxygen available for respiration and increasing the nitrate loss by denitrification.

The heaving of isopycnals associated with ENSO partially explains the remarkable shoaling and upward expansion of the upper part of AAIW observed in the southern part of the section, with AAIW replacing ESSW between 150 and 500 m. This fact brought a large increase in advected oxygen to this depth range of the OMZ during 2009, which led to larger consumption of oxygen through increased respiration, and to larger production of remineralized nitrate. Therefore, at an interannual time scale, the upward movement of isopycnals associated with La Niña conditions favors the ventilation of the OMZ by AAIW.

We have shown that the shoaling of AAIW is also partially explained by the fact that AAIW flowed along shallower isopycnals in 2009. This is in good agreement with the long-term trend of shoaling and density reductions of the core of AAIW as found by Schmidtko and Johnson (2012) south of 15° S in the eastern South Pacific. At an interdecadal time scale, such changes in the pattern of advection of AAIW may mitigate the long-term trend of expanding OMZs found in the world ocean (Stramma et al., 2008), possibly explaining why an increase in oxygen content has been reported for some areas of the subtropical gyres, e.g. off Chile between 200 and 700 m (see Fig. 2d of Stramma et al., 2010b). However, the temporal resolution of our data set prevents us from testing this hypothesis.

Besides the general changes described above, we have observed a few cores along the latitudinal section in which oxygen and nitrate change in a distinct way. These cores are related to changes in the intensity of the zonal currents of the equatorial current system. The eastward flowing currents ventilate the OMZ, as they supply waters with a relatively higher oxygen content, whereas the westward flowing currents transport waters almost depleted of oxygen from the OMZ. Therefore, a weakening of an eastward (or a strengthening of a westward) current enhances the presence of ESSW and brings about a decrease / an increase in advected oxygen/nitrate; this leads to a decrease in the respired oxygen and in the remineralized nitrate, and may induce further nitrate loss by denitrification. The situation reverses with a strengthening of the eastward currents or a weakening of the westward currents.

Supplementary material related to this article is available online at http://www.biogeosciences.net/10/6339/2013/bg-10-6339-2013-supplement.pdf.

Acknowledgements. We are very grateful to the anonymous reviewers who provided constructive and useful comments which certainly helped to improve this manuscript. P. J. Llanillo was supported through a JAE grant from Consejo Superior de Investigaciones Científicas and the European Social Fund. Financial support was received through Laboratorio Internacional de Cambio Global CSIC/PUC (P. J. Llanillo and J. L. Pelegrí), project TIC-MOC (CTM2011-28867) funded by the Spanish Ministerio de Ciencia e Innovación (P. J. Llanillo and J. L. Pelegrí), GEOMAR Helmholtz Centre for Ocean Research Kiel (J. Karstensen and L. Stramma) and DFG-supported project SFB 754 (www.sfb754.de) (J. Karstensen and L. Stramma).

Edited by: A. Paulmier

References

Anderson, L. A. and Sarmiento, J. L.: Redfield ratios of remineralization determined by nutrient data analysis, Global Biogeochem. Cy., 8, 65–80, 1994.

Barber, R. T. and Chavez, F. P.: Biological consequences of El Niño, Science, 222, 1203–1210, 1983.

Bindoff, N. L. and McDougall, T. J.: Diagnosing climate change and ocean ventilation using hydrographic data, J. Phys. Oceanogr., 24, 1137–1152, 1994.

Brink, K. H., Halpern, D., Huyer, A., and Smith, R. L.: The physical environment of the Peruvian upwelling system, Progr. Oceanogr., 12, 285–305, 1983.

Chavez, F. P., Ryan, J., Lluch-Cota, S. E., and Ñiquen C, M.: From anchovies to sardines and back: multidecadal change in the Pacific Ocean, Science, 299, 217–221, 2003.

Chavez, F. P., Bertrand, A., Guevara-Carrasco, R., Soler, P., and Csirke, J.: The northern Humboldt Current System: Brief history, present status and a view towards the future, Progr. Oceanogr., 79, 95–105, 2008.

Codispoti, L. A., Brandes, J. A., Christensen, J. P., Devol, A. H., Naqvi, S. W. A., Paerl, H. W., and Yoshinari, T.: The oceanic fixed nitrogen and nitrous oxide budgets: Moving targets as we enter the anthropocene?, Scientia Marina, 65, 85–105, 2001.

Czeschel, R., Stramma, L., Schwarzkopf, F. U., Giese, B. S., Funk, A., and Karstensen, J.: Middepth circulation of the eastern tropical South Pacific and its link to the oxygen minimum zone, J. Geophys. Res., 116, C01015, doi:10.1029/2010JC006565, 2011.

Czeschel, R., Stramma, L., and Johnson, G. C.: Oxygen decreases and variability in the eastern equatorial Pacific, J. Geophys. Res., 117, C11019, doi:10.1029/2012JC008043, 2012.

De Pol-Holz, R., Ulloa, O., Lamy, F., Dezileau, L., Sabatier, P., and Hebbeln, D.: Late quaternary variability of sedimentary nitrogen isotopes in the eastern South Pacific Ocean, Paleoceanography, 22, PA2207, doi:10.1029/2006PA001308, 2007.

Deutsch, C., Brix, H., Ito, T., Frenzel, H., and Thompson, L.: Climate-forced variability of ocean hypoxia, Science, 333, 336–339, 2011.

Fiedler, P. C. and Talley, L. D.: Hydrography of the eastern tropical Pacific: A review, Progr. Oceanogr., 69, 143–180, doi:10.1016/j.pocean.2006.03.008, 2006.

Garcia, H. E. and Gordon, L. I. : Oxygen solubility in seawater: Better fitting equations. Limnol. Oceanogr., 37, 1307–1312, 1992.

Grasse, P., Stichel, T., Stumpf, R., Stramma L., and M. Frank, M.: The distribution of neodymium isotopes and concentrations in the Eastern Equatorial Pacific: Water mass advection versus particle exchange, Earth Planet. Sci. Lett., 353/354, 198–207, 2012.

Gruber, N. and Sarmiento, J. L.: Global patterns of marine nitrogen fixation and denitrification, Global Biogeochem. Cy., 11, 235–266, 1997.

Guillén, O., Cárcamo, E., and Calientes, R.: Oxígeno disuelto, nutrientes y clorofila frente a la costa peruana durante El Niño 1987, Memorias del Simposio Internacional de los Recursos Vivos y las Pesquerías en el Pacífico Sud-Este. Rev. Comisión Permanente del Pacífico Sur., Número especial, 83–94, 1988.

Hamersley, M. R., Lavik, G., Woebken, D., Rattray, J. E., Lam, P., Hopmans, E. C., Sinninghe Damsté, J. S., Krüger, S., Graco, M., Gutiérrez, D., and Kuypers, M. M. M.: Anaerobic ammonium oxidation in the Peruvian oxygen minimum zone, Limnol. Oceanogr., 52, 923–933, 2007.

Hartin, C. A., Fine, R. A., Sloyan, B. M., Talley, L. D., Chereskin, T. K., and Happell, J.: Formation rates of Subantarctic mode water and Antarctic intermediate water within the South Pacific, Deep Sea Res. Pt. I, 58, 524–534, 2011.

Holte, J. W., Talley, L. D., Chereskin, T. K., and Sloyan, B. M.: The role of air-sea fluxes in Subantarctic Mode Water formation, J. Geophys. Res., 117, C03040, doi:10.1029/2011JC007798, 2012.

Hupe, A. and Karstensen, J.: Redfield stoichiometry in Arabian Sea subsurface waters, Global Biogeochem. Cy., 14, 357–372, 2000.

Johnson, G. C., Sloyan, B. M., Kessler, W. S., and McTaggart, K. E.: Direct measurements of upper ocean currents and water properties across the tropical Pacific during the 1990s, Progr. Oceanogr., 52, 31–61, 2002.

Kalvelage, T., Jensen, M. M., Contreras, S., Revsbech, N. P., Lam, P., Günter, M., LaRoche, J., Lavik, G., and Kuypers, M. M. M.: Oxygen sensitivity of anammox and coupled N-cycle processes in oxygen minimum zones, PLoS ONE, 6, e29299, doi:10.1371/journal.pone.0029299, 2011.

Karstensen, J.: Formation of the South Pacific shallow salinity minimum: A Southern Ocean pathway to the tropical Pacific, J. Phys. Oceanogr., 34, 2398–2412, 2004.

Karstensen, J. and Tomczak, M.: Age determination of mixed water masses using CFC and oxygen data, J. Geophys. Res., 103, 18599–18609, 1998.

Karstensen, J., Stramma, L., and Visbeck, M.: Oxygen minimum zones in the eastern tropical Atlantic and Pacific oceans, Progr. Oceanogr., 77, 331–350, 2008.

Kessler, W. S.: The circulation of the eastern tropical Pacific: A review, Progr. Oceanogr., 69, 181–217, 2006.

Kuypers, M. M. M., Lavik, G., Woebken, D., Schmid, M., Fuchs, B. M., Amann, R., Jørgensen, B. B., and Jetten, M. S. M.: Massive nitrogen loss from the Benguela upwelling system through anaerobic ammonium oxidation, P. Natl. Acad. Sci. USA, 102, 6478–6483, 2005.

Lam, P., Lavik, G., Jensen, M. M., van de Vossenberg, J., Schmid, M., Woebken, D., Gutiérrez, D., Amann, R., Jetten, M. S. M., and Kuypers, M. M. M.: Revising the nitrogen cycle in the Peruvian oxygen minimum zone, P. Natl. Acad. Sci. USA, 106, 4752–4757, doi:10.1073/pnas.0812444106, 2009.

Lipschultz, F., Wofsy, S. C., Ward, B. B., Codispoti, L. A., Friedrich, G., and Elkins, J. W.: Bacterial transformations of inorganic nitrogen in the oxygen-deficient waters of the Eastern Tropical South Pacific Ocean, Deep Sea Res. Pt A., 37, 1513–1541, 1990.

Llanillo, P. J., Pelegrí, J. L., Duarte, C. M., Emelianov, M., Gasser, M., Gourrion, J., and Rodríguez-Santana, A.: Meridional and zonal changes in water properties along the continental slope off central and northern Chile, Ciencias Marinas; Vol. 38, No. 1B: Special issue on Descriptive Oceanography with Tracers in Coastal and Deep Oceans, 307–332, 2012.

Mackas, D. L., Denman, K. L., and Bennett, A. F.: Least squares multiple tracer analysis of water mass composition, J. Geophys. Res., 92, 2907–2918, 1987.

Mantua, N. J., Hare, S. R., Zhang, Y., Wallace, J. M., and Francis, R. C.: A Pacific interdecadal climate oscillation with impacts on salmon production, B Am. Meteorol. Soc., 78, 1069–1079, 1997.

Morales, C., Hormazábal, S., and Blanco, J. L.: Interannual variability in the mesoscale distribution of the depth of the upper boundary of the oxygen minimum layer off northern Chile (18–24° S): Implications for the pelagic system and biogeochemical cycling, J. Mar. Res., 57, 909–932, 1999.

Paulmier, A. and Ruiz-Pino, D.: Oxygen minimum zones (OMZs) in the modern ocean, Progr. Oceanogr., 80, 113–128, doi:10.1016/j.pocean.2008.08.001, 2009.

Paulmier, A., Ruiz-Pino, D., Garçon, V., and Farías L.: Maintaining of the East South Pacific Oxygen Minimum Zone (OMZ) off Chile, Geophys. Res. Lett., 33, L20601, doi:10.1029/2006GL026801, 2006.

Philander, S. G. H.: El Niño Southern Oscillation phenomena, Nature, 302, 295–301, 1983.

Poole, R. and Tomczak, M.: Optimum multiparameter analysis of the water mass structure in the Atlantic Ocean thermocline, Deep Sea Res. Pt. I, 46, 1895–1921, 1999.

Redfield, A. C., Ketchum, B. H., and Richards, F. A.: The influence of organisms on the composition of sea-water, in: The Sea: ideas and observations on progress in the study of the seas (vol. 2), edited by: Hill, M. N., Wiley, London, 26–77, 1963.

Reid, J. L.: The shallow salinity minima of the Pacific Ocean, Deep Sea Res., 20, 51–68, 1973.

Roemmich, D., Gilson, J., Davis, R., Sutton, P., Wijffels, S., and Riser, S.: Decadal spinup of the South Pacific Subtropical Gyre, J. Phys. Oceanogr., 37, 162–173, 2007.

Schmidtko, S. and Johnson, G. C.: Multidecadal warming and shoaling of Antarctic Intermediate Water, J. Climate, 25, 207–221, 2012.

Silva, N., Rojas, N., and Fedele, A.: Water masses in the Humboldt Current System: Properties, distribution, and the nitrate deficit as a chemical water mass tracer for Equatorial Subsurface Water off Chile, Deep Sea Res. PtII, 56, 1004–1020, 2009.

Stramma, L., Peterson, R. G., and Tomczak, M.: The South Pacific Current, J. Phys. Oceanogr., 25, 77–91, 1995.

Stramma, L., Johnson, G. C., Sprintall, J., and Mohrholz, V.: Expanding oxygen-minimum zones in the Tropical Oceans, Science, 320, 655–658, 2008.

Stramma, L., Johnson, G. C., Firing, E., and Schmidtko, S.: Eastern Pacific oxygen minimum zones: supply paths and multidecadal changes, J. Geophys. Res., 115, C09011, doi:10.1029/2009JC005976, 2010a.

Stramma, L., Schmidtko, S., Levin, L. A., and Johnson, G. C.: Ocean oxygen minima expansions and their biological impacts, Deep Sea Res. Pt. I, 57, 587–595, 2010b.

Stramma, L., Prince, E. D., Schmidtko, S., Luo, J., Hoolihan, J. P., Visbeck, M., Wallace, D. W. R., Brandt, P., and Kortzinger, A.: Expansion of oxygen minimum zones may reduce available habitat for tropical pelagic fishes, Nature Clim. Change, 2, 33–37, 2012.

Stramma, L., Bange, H. W., Czeschel, R., Lorenzo, A., and Frank, M.: On the role of mesoscale eddies for the biological productivity and biogeochemistry in the eastern tropical Pacific Ocean off Peru, Biogeosciences Discuss., 10, 9179–9211, doi:10.5194/bgd-10-9179-2013, 2013.

Strub, P., Mesias, J., Montecino, V., Rutllant, J., and Salinas, S.: Coastal ocean circulation off western South America, in: The Sea: The global coastal ocean, edited by: Robinson, A. and Brink, K. H., Wiley, New York, 272–313, 1998.

Thamdrup, B., Dalsgaard, T., Jensen, M. M., Ulloa, O., Farías, L., and Escribano, R.: Anaerobic ammonium oxidation in the oxygen-deficient waters off northern Chile, Limnol. Oceanogr., 51, 2145–2156, 2006.

Tomczak, M. and Large, D. G. B.: Optimum multiparameter analysis of mixing in the thermocline of the Eastern Indian Ocean, J. Geophys. Res., 94, 16141–16149, 1989.

Tsuchiya, M. and Talley, L. D.: A Pacific hydrographic section at 88° W: Water-property distribution, J. Geophys. Res., 103, 12899–12918, 1998.

Vaquer-Sunyer, R. and Duarte, C. M.: Thresholds of hypoxia for marine biodiversity, P. Natl. Acad. Sci. USA, doi:10.1073/pnas.0803833105, 2008.

Wyrtki, K.: Circulation and water masses in the eastern equatorial Pacific Ocean, Int. J. Oceanol. Limnol., 1, 117–147, 1967.